

Directly growing hierarchical nickel-copper hydroxide nanowires on carbon fibre cloth for efficient electrooxidation of ammonia

Xu, W, Lan, R, Du, D, Humphreys, J, Walker, M, Wu, Z, Wang, H & Tao, S

Published PDF deposited in Coventry University's Repository

Original citation:

Xu, W, Lan, R, Du, D, Humphreys, J, Walker, M, Wu, Z, Wang, H & Tao, S 2017, 'Directly growing hierarchical nickel-copper hydroxide nanowires on carbon fibre cloth for efficient electrooxidation of ammonia' *Applied Catalysis B: Environmental*, vol 218, pp. 470-479

<https://dx.doi.org/10.1016/j.apcatb.2017.07.005>

DOI 10.1016/j.apcatb.2017.07.005

ISSN 0926-3373

Publisher: Elsevier

This is an open access article under the CC BY license
(<http://creativecommons.org/licenses/by/4.0/>).

Copyright © and Moral Rights are retained by the author(s) and/ or other copyright owners. A copy can be downloaded for personal non-commercial research or study, without prior permission or charge. This item cannot be reproduced or quoted extensively from without first obtaining permission in writing from the copyright holder(s). The content must not be changed in any way or sold commercially in any format or medium without the formal permission of the copyright holders.



Directly growing hierarchical nickel-copper hydroxide nanowires on carbon fibre cloth for efficient electrooxidation of ammonia

Wei Xu^{a,b}, Rong Lan^a, Dongwei Du^a, John Humphreys^a, Marc Walker^c, Zucheng Wu^b, Huanting Wang^d, Shanwen Tao^{a,d,*}

^a School of Engineering, University of Warwick, Coventry CV4 7AL, UK

^b Department of Environmental Engineering, State Key Laboratory of Clean Energy Utilization, Zhejiang University, Hangzhou 310058, Zhejiang, China

^c Department of Physics, University of Warwick, Coventry CV4 7AL, UK

^d Department of Chemical Engineering, Monash University, Clayton, Victoria 3800, Australia

ARTICLE INFO

Article history:

Received 17 February 2017

Received in revised form 28 June 2017

Accepted 3 July 2017

Available online 4 July 2017

Keywords:

Hierarchical
Layered hydroxide
Electrocatalyst
Nano-wire
Ammonia oxidation

ABSTRACT

Ammonia is an attractive carbon-free chemical for electrochemical energy conversion and storage. However, the sluggish kinetic rates of the ammonia electrooxidation reaction, and high cost and poisoning of Pt-based catalysts still remain challenges. This also limits the development of direct ammonia fuel cells. In this work, we directly grew hierarchical mixed NiCu layered hydroxides (LHS) nanowires on carbon fibre cloth electrodes by a facile one-step hydrothermal synthesis method for efficient electro-oxidation of ammonia. This catalyst achieves a current density of 35 mA cm⁻² at 0.55 V vs. Ag/AgCl, which is much higher than that of bare Ni(OH)₂ catalyst (5 mA cm⁻²). This is due to abundant active sites and a synergistic effect between Ni and Cu, possibly due to the formation of Ni_{1-x}Cu_xOOH on the surface of the catalysts through the electrochemical activation of the mixture of Cu(OH)₂ and α-Ni(OH)₂. In the investigated first row transition elements, it is found that Cu is the sole first-row transition metal to effectively improve activity of Ni(OH)₂ for ammonia electrooxidation. This mixed NiCu LHS nano-wire catalyst outperforms commercial Pt/C catalyst in the aspects of ammonia oxidation current and stability, demonstrating it to be a promising low-cost and stable catalyst for efficient ammonia electrooxidation in alkaline condition, which is a potential electrode for ammonia fuel cells for power generation or electrolysis of ammonia for ammonia-containing wastewater treatment.

© 2017 The Author(s). Published by Elsevier B.V. This is an open access article under the CC BY license (<http://creativecommons.org/licenses/by/4.0/>).

1. Introduction

Ammonia is regarded as a carbon-free hydrogen-storage material with a hydrogen weight percent of 17.6 wt% [1–3]. Direct electrooxidation of ammonia at room temperature has wide applications in energy conversion and storage such as direct ammonia fuel cells and hydrogen fuel production [4–7]. In theory, the energy required in ammonia electrolysis (0.06 V) is 95% less than the required energy cost in water electrolysis (1.23 V) for hydrogen production [8]. Besides, it is also a promising technology to remove nitrogen for wastewater remediation [8]. However, the main challenge of ammonia electrooxidation is sluggish kinetic rates. Until now, Pt and Pt-based catalysts for ammonia electrooxidation have been extensively investigated due to their low

overpotential [9–14]. However, the ammonia poisoning and high price of Pt still remain a barrier for its large-scale application [15].

Due to the challenges listed above, many research works aim to develop Pt-free catalysts with high activity and stability for use in the ammonia electrode [15]. Nickel is a much more earth-abundant and therefore affordable to use as an electrode material for electrochemical devices. However, it has been found that it is inactive toward ammonia electrooxidation [16,17]. Nevertheless, Kapařka et al. discovered that ammonia could be catalytically oxidized on Ni(OH)₂, which was generated through the electrooxidation of the Ni electrode in alkaline conditions [18]. They explained that the ammonia electrooxidation on Ni(OH)₂ was attributed to the electrocatalytic reaction on NiOOH, which could be formed via a reversible electrochemical reaction between Ni(OH)₂ and NiOOH [19,20]. Although Ni(OH)₂ shows good catalytic property as a Pt-free electrode, it still has disadvantages such as electrode stability and the concomitant release of Ni to the electrolyte [18].

Transition metal based electrocatalysts and metal-organic electrocatalysts have been reported to be promising alternatives to

* Corresponding author at: School of Engineering, University of Warwick, Coventry CV4 7AL, UK.

E-mail address: S.Tao.1@warwick.ac.uk (S. Tao).

noble metals [21,22]. Recently, the first-row transition metal based layered hydroxides (LHs) with brucite like layers have attracted much attention in electrochemical energy applications [23–27]. Among them, nickel based LHs have been widely investigated in water electrolysis in alkaline conditions. The catalytic activity of Ni-based LHs is largely dependent on the doping element. So far, NiFe and NiV LHs have proven to show the best catalytic performance in water electrolysis [28–30]. Other dopants, including Mn and Cr, can also improve catalytic active but to a lesser extent than Fe and V [24]. Contrary to the promotion observed from other dopants, the incorporation of Co, Cu and Zn has been shown to reduce the catalytic activity to electrolysis of water [24].

Although it has been reported that pure $\text{Ni}(\text{OH})_2$ has good catalytic activity to electrochemical oxidation of ammonia [18], to the best of our knowledge, reports on Ni-based LHs for ammonia electrooxidation are scarce. Introduction of another element in layered hydroxides will significantly change the catalytic properties as described above. In a recent study, we found that NiCu bimetal exhibit excellent catalytic activity toward electrochemical oxidation of ammonia [31]. Actually, we found that after electrochemical activation NiCu would be transformed from bimetal to hydroxides, which were the final effective catalysts. In this study, instead of preparing bimetal, we directly prepare the hydroxides, i.e., the real active catalysts through a facile hydrothermal synthesis process. It was found that the nickel copper hydroxides still exhibit the best catalytic activity, and the oxidation current density was improved when compared to nickel copper bimetal, which further confirm nickel copper hydroxide is an excellent catalyst for electrochemical oxidation of ammonia. Here we choose Cu as the dopant in order to prepare NiCu LHs. Cu was chosen as it is theoretically predicted to be one of the most active metals for ammonia electrooxidation [32]. Although previous work shows bare Cu is almost inactive toward ammonia electrooxidation as Cu binds N atoms too weakly leading to a very high overpotential [33], NiCu LHs are expected to perform well due to a synergistic effect between Cu and Ni, since Ni binds N atoms strongly [32]. In this work, we synthesised hierarchical NiCu LHs with nano-wires structure on carbon fibre cloth via a facile hydrothermal reaction followed by electrochemical activation but the final products are a mixture of $\text{Cu}(\text{OH})_2$ and $\text{Ni}(\text{OH})_2$. The mixed layered $\text{Cu}(\text{OH})_2$ and $\text{Ni}(\text{OH})_2$ catalysts could be converted into $\text{Ni}_{1-x}\text{Cu}_x\text{OOH}$ by electrochemical activation, which shows much higher activity than pure $\text{Ni}(\text{OH})_2$ catalyst, and even outperform the commercial Pt/C catalyst. For comparison, other first-row transition metals including Cr, Mn, Fe, Co, Zn are also used as dopants to prepare Ni-based LHs respectively. It was found that, among these elements, Cu is the unique element which can significantly improve catalytic activity towards electrooxidation of ammonia. The synthesised nickel-copper hydroxide also exhibit hierarchical microstructure which can maximise the surface area to further increase the catalytic activity [34,35].

2. Experimental section

2.1. Materials

Nickel(II) nitrate hexahydrate ($\text{Ni}(\text{NO}_3)_2 \cdot 6\text{H}_2\text{O}$, 98%, Alfa Aesar), and copper(II) nitrate hemi(pentahydrate) ($\text{Cu}(\text{NO}_3)_2 \cdot 2.5\text{H}_2\text{O}$, 99.0%, Alfa Aesar) were utilized without any further purification. Plain carbon fibre cloth (0.35 mm thickness, E-TEK) was used as substrate for the catalysts. Carbon fibre cloth electrode ($1 \times 3 \text{ cm}^2$) was first cleaned using HCl and ethanol, before being rinsed with deionized water as a pre-treatment before the hydrothermal reaction in an autoclave. Nafion® solution (5 wt%) were purchased from Sigma-Aldrich. Other chemicals including $\text{Cr}(\text{NO}_3)_3 \cdot 9\text{H}_2\text{O}$, $\text{Mn}(\text{NO}_3)_2 \cdot 4\text{H}_2\text{O}$, $\text{Fe}(\text{NO}_3)_3 \cdot 9\text{H}_2\text{O}$, $\text{Co}(\text{NO}_3)_2 \cdot 6\text{H}_2\text{O}$, $\text{Zn}(\text{NO}_3)_3 \cdot 6\text{H}_2\text{O}$,

NH_4Cl , urea, isopropanol and NaOH were all analytical reagents and bought from Alfa Aesar. Pt/C (20 wt%) was also bought from Alfa Aesar.

2.2. Preparation of Ni-based LHs

Hierarchical nickel-copper LHs were directly formed on a carbon fibre cloth (CFC) electrode via a one-step hydrothermal method. Briefly, 20 mL of metal precursor solution consisting of Ni^{2+} and Cu^{2+} ions was prepared by mixing $\text{Ni}(\text{NO}_3)_2 \cdot 6\text{H}_2\text{O}$ and $\text{Cu}(\text{NO}_3)_2 \cdot 2.5\text{H}_2\text{O}$ in deionized water. To study the effect of Cu proportion, different mole ratios of $\text{Ni}^{2+}/\text{Cu}^{2+}$ metal precursor solution (1:0, 9:1, 4:1, 7:3, 3:2 and 1:1, with correspondingly obtained samples named bare $\text{Ni}(\text{OH})_2$, $\text{Ni}_{0.9}\text{Cu}_{0.1}$ LHs, $\text{Ni}_{0.8}\text{Cu}_{0.2}$ LHs, $\text{Ni}_{0.7}\text{Cu}_{0.3}$ LHs, $\text{Ni}_{0.6}\text{Cu}_{0.4}$ LHs and $\text{Ni}_{0.5}\text{Cu}_{0.5}$ LHs, respectively) were employed, while the total amount of metal ions (Ni^{2+} and Cu^{2+}) was kept at 1 mmol. 75 mg of urea was then added to the aqueous mixed metal nitrate solution. After stirring for 10 min, the mixture solution was transferred to a Teflon-lined stainless steel autoclave. The carbon fibre cloth electrode was then soaked in the solution, followed by heating at 120 °C for 14 h in an oven. The as-synthesised electrodes were washed using deionized water and ethanol four times, after which they were then dried at 60 °C in a vacuum oven overnight. The catalyst loading on the electrode was calculated by the weight difference of carbon fibre cloth electrode after and before hydrothermal synthesis.

In this work, other transition metals were also used to prepare NiM LHs (M = Cr, Mn, Fe, Co, Zn, respectively). In order to synthesise the NiM LHs a similar method to that of NiCu LHs was used with copper nitrate replaced by other metal nitrates. All the mole ratios of Ni/M in the metal precursor solutions were fixed to 1:1.

For comparison, carbon supported Pt (Pt/C) particles were ultrasonically dispersed in a mixture of Nafion® solution, isopropanol and deionized water in order to get the catalysts ink. It was then brushed onto a carbon fibre cloth electrode to prepare Pt/C electrodes for comparison. The Pt loading on the carbon fibre electrode was 0.4 mg cm⁻² [36].

2.3. Characterization

X-ray diffraction (XRD) analysis (Panalytical X-Pert Pro MPD with Cu K α 1 radiation) was used to examine the phases of the samples. X-ray photoelectron spectroscopy (XPS) data were collected using a Kratos Axis Ultra DLD spectrometer (Kratos Analytical, UK), with samples being illuminated using an Al K α x-ray source and photoelectrons collected using the detector at a resolution of approximately 0.4 eV. A charge neutraliser was used to negate the effects of differential charging of the surface during the experiment, with binding energies subsequently referenced to the C 1s energy level at 284.85 eV. The microstructure and morphology were examined using a scanning electron microscope (SEM, Zeiss SUPRA 55-VP) equipped with an energy-dispersive X-ray (EDX) spectrometer that allows elemental composition analysis. Transmission electron microscopy (TEM) was conducted by using JEOL 2100.

Electrochemical characterization was performed in a three-electrode system at room temperature, where the catalyst coated carbon fibre electrode was the working electrode, Pt foil was used as the counter electrode and Ag/AgCl as the reference electrode. All electrodes were connected to a Solartron 1287A electrochemical station in order to conduct the electrochemical measurements. Before testing, all samples were electrochemically activated by potential cycling between -0.2 V and 1.0 V vs. Ag/AgCl (200 scans), at 50 mV s⁻¹ of scan rate in 0.5 M NaOH at room temperature. The cyclic voltammetry (CV) measurements, from 0 V to 0.8 V with a scan rate of 25 mV s⁻¹, were recorded after at least 3 cycles to

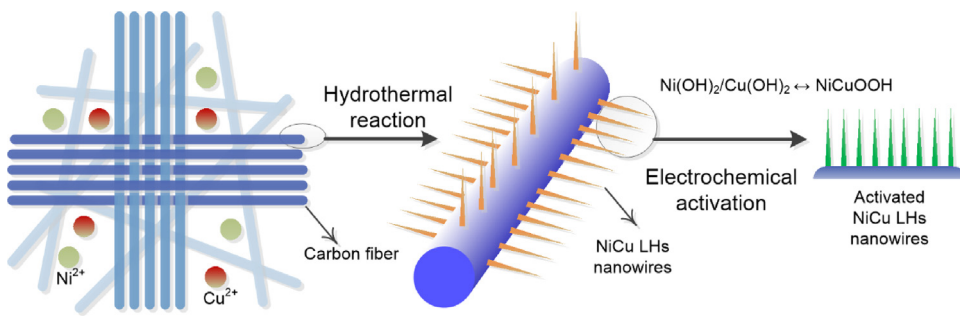


Fig. 1. Schematic diagram of catalyst preparation for growing NiCu LHS nanowires on carbon fibre cloth electrode and subsequent electrochemical activation of NiCu LHS.

get stable results in 0.5 M NaOH with the absence and presence of 55 mM NH_4Cl . The linear sweep voltammetry (LSV) was measured from 0.2 to 0.7 V versus Ag/AgCl with a slow scan rate of 2 mV s⁻¹ under stirring.

2.4. Ions measurement and capacitance calculation

Ammonium and nitrate ions were detected by ion chromatography (Metrohm® 883 IC, with Metrosep C 4 – 250/4.0 column for cations and ICsep AN2 column for anions) using an electrical conductivity detector. To determine the molar ratio of Ni:Cu on the CFC, the CFC samples were immersed in 0.1 M HCl overnight to dissolve the Ni and Cu hydroxides. Then the amount Ni and Cu ions were detected by ion chromatography. The specific pseudocapacitance, C (F g⁻¹), of catalyst was evaluated from CV plots through the following equation:

$$C = \frac{1}{m\nu\Delta V} \int i(V)dV \quad (1)$$

where m was the mass loading of catalyst on carbon fibre electrode (g), ν was the scan rate for the CV measurement (V s⁻¹), ΔV was the potential range (V), and $i(V)$ was the current response (A) at potential V (V) [37].

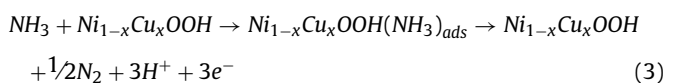
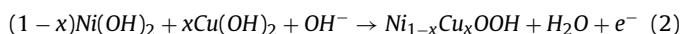
3. Results and discussion

3.1. Preparation and characterization of NiCu LHS

The hierarchical NiCu LHS nanowires were directly grown on commercial carbon fibre cloth (CFC) by a hydrothermal route first and then with an electrochemical treatment, as schematically elucidated in Fig. 1. During the reaction process, nickel and copper ions were precipitated under basic conditions from progressive hydrolysis of urea to produce bulk NiCu LHS sediment; meanwhile some $\text{Ni}_{1-x}\text{Cu}_x$ LHS (x was copper percent of total metals in the precursor solution of hydrothermal reaction) were attached onto the surface of CFC to form nanowires. In Fig. 2a, hybrid Cu(OH)_2 phase (JCPDS 00-035-0505) and $\alpha\text{-Ni(OH)}_2$ phase (JCPDS 00-022-0444) [38] with layered structure were observed in the XRD patterns of targeting NiCu LHS grown on CFC before electrochemical activation. This indicates that the initial products are a mixture of Cu(OH)_2 and $\alpha\text{-Ni(OH)}_2$, both exhibit layered structure. On the other hand, the bare Ni(OH)_2 growing on carbon fibre obtained pure hexagonal $\alpha\text{-Ni(OH)}_2$ phase (JCPDS 00-022-0444) supported by the XRD pattern in Fig. 2a.

The as-prepared NiCu LHS and bare Ni(OH)_2 catalysts had few active sites, hence an electrochemical treatment was conducted to enhance the activity before electrochemical tests. NiCu LHS coated carbon fibre cloth was scanned over 200 cycles from a potential of -0.2 V to 1.0 V vs. Ag/AgCl in NaOH, the records were shown in Fig. S1 (Supporting Information). During the 1st cycle, there was no anodic peak observed. After the 1st cycle, a pair of small redox

peaks appeared. As the number of cycles increased, the redox peaks became larger and larger, finally becoming stable at around the 200th cycle. These redox peaks were attributed to the transformation between NiCu hydroxides (mixed Cu(OH)_2 and $\alpha\text{-Ni(OH)}_2$) and NiCu oxyhydroxide ($\text{Ni}_{1-x}\text{Cu}_x\text{OOH}$ or, mixed NiOOH and CuOOH) [24,31]. Larger redox peaks meant a larger pseudocapacitance from reversible conversion of oxidative state and reductive state due to more activated $\text{Ni}_{1-x}\text{Cu}_x\text{OOH}$ sites on the catalyst surface. For the 1st cycle, there were two reduction peaks indicating the reduction of formed NiOOH and CuOOH respectively. However, after the 10th cycle, only one reduction peak was remained, indicating the possible formation of $\text{Ni}_{1-x}\text{Cu}_x\text{OOH}/\text{Ni}_{1-x}\text{Cu}_x(\text{OH})_2$. In order to study the electrocatalytic mechanism, XPS of Ni-Cu hydroxides before and after electrocatalysis was carried out. In Fig. 2c, Ni^{2+} and Ni^{3+} of Ni element on the catalyst surface were observed, which were bound to oxygen [39,40]. Fig. 2d shown that Cu element existed as Cu_2O and Cu(OH)_2 . The $\text{Cu(OH)}_2/\text{Cu}_2\text{O}$ ratio increased after electrocatalysis. Interestingly, there was a general shift in the Ni binding energies after electrocatalysis, moving downward around 1.0 eV as shown in Fig. 2c. For example, the Ni^{3+} peak centered at 856.16 eV before electrocatalysis shifted to 855.16 eV after electrocatalysis. This was possibly due to the formation of NiCu double hydroxide ($\text{Ni}_{1-x}\text{Cu}_x(\text{OH})_2$) and/or oxyhydroxides ($\text{Ni}_x\text{Cu}_{1-x}\text{OOH}$) in alkaline solution [31]. According to the mechanism of ammonia electrooxidation on Ni(OH)_2 -based catalysts [18]:



It is believed that ammonia was oxidized via a direct electron transfer from the adsorbed NH_3 to the $\text{Ni}_{1-x}\text{Cu}_x\text{OOH}$ catalyst. Accordingly, increasing $\text{Ni}_{1-x}\text{Cu}_x\text{OOH}$ sites by electrochemical activation proved to be a very important factor for optimizing catalysts in the ammonia oxidation reaction, as it was well known that an increase in the number of active sites often led to an enhancement of the catalytic activity. After electrochemical activation, it was observed that the colour of hierarchical NiCu LHS changed from green to black. XRD patterns of catalysts after electrochemical activation are shown in Fig. 2a. Both bare Ni(OH)_2 and NiCu LHS were observed to have some changes. A (001) peak of $\beta\text{-Ni(OH)}_2$ was newly added at 2 θ degree of 19° for bare Ni(OH)_2 , indicating some $\alpha\text{-Ni(OH)}_2$ had been changed to $\beta\text{-Ni(OH)}_2$ (JCPDS 00-014-0117) [41] via potential cycling in alkaline condition. It should be noted that ageing of $\alpha\text{-Ni(OH)}_2$ can also lead to the formation of $\beta\text{-Ni(OH)}_2$ [42]. It is very likely the loss of water from $\alpha\text{-Ni(OH)}_2$ happened leading to the formation of $\beta\text{-Ni(OH)}_2$ when the sample was taken out from the solution for XRD analyses. The loss of water and structure change from $\alpha\text{-Ni(OH)}_2$ to $\beta\text{-Ni(OH)}_2$ is shown in Fig. 2b. For NiCu LHS, the (020) peak of Cu(OH)_2 at 2 θ degree

of 17° and (002) peak of $\alpha\text{-Ni(OH)}_2$ at 2θ degree of 22° , which were observed before electrochemical activation, have almost disappeared at this stage. However, the bulk of NiCu LHS still composed of Cu(OH)_2 and $\alpha\text{-Ni(OH)}_2$ after the electrochemical activation. Single phase layered double hydroxide might have been formed, but it could be transformed to Cu(OH)_2 and $\beta\text{-Ni(OH)}_2$ due to loss of water after taking out from the liquid electrolyte for XRD analysis.

SEM image of bare Ni(OH)_2 /carbon fibre electrode is shown in Fig. 3a. The carbon fibre tubes were tightly covered with hierarchical Ni(OH)_2 nanosheets. Besides, some excess Ni(OH)_2 aggregated in to bulk balls with a diameter of $2\text{-}3 \mu\text{m}$ and then attached to the carbon fibres. The as-prepared nominal $\text{Ni}_{0.8}\text{Cu}_{0.2}$ LHS with real composition of a mixture of Cu(OH)_2 and $\alpha\text{-Ni(OH)}_2$ directly grown on carbon fibre cloth via hydrothermal synthesis has a hierarchical nanowire microstructure with a length of $1\text{-}2 \mu\text{m}$, as shown in Fig. 3b. The atom ratio of Ni/Cu in $\text{Ni}_{0.8}\text{Cu}_{0.2}$ LHS was about $2/1$ according to energy-dispersive X-ray (EDX) spectrum (in Fig. S2). To verify the Ni/Cu ratio, metal hydroxides were dissolved in HCl, and then measured by ion chromatography. The obtained Ni/Cu ratio was $1.9:1$, very close to the result of EDX. In the following text, we still use symbol $\text{Ni}_{0.8}\text{Cu}_{0.2}$ LHS to represent the composition of the starting precursor for preparation of the sample although there is a deviation on the final real composition. SEM images of other nominal NiCu LHS samples (i.e. $\text{Ni}_{0.9}\text{Cu}_{0.1}$ LHS, $\text{Ni}_{0.7}\text{Cu}_{0.3}$ LHS, $\text{Ni}_{0.6}\text{Cu}_{0.4}$ LHS, $\text{Ni}_{0.5}\text{Cu}_{0.5}$ LHS) grown on carbon fibre cloth electrodes are shown in Fig. S3 of Supporting Information. The NiCu LHS nanowires after electrochemical tests with diameter of $20\text{-}25 \text{ nm}$ were further observed by TEM as shown in Fig. 3c.

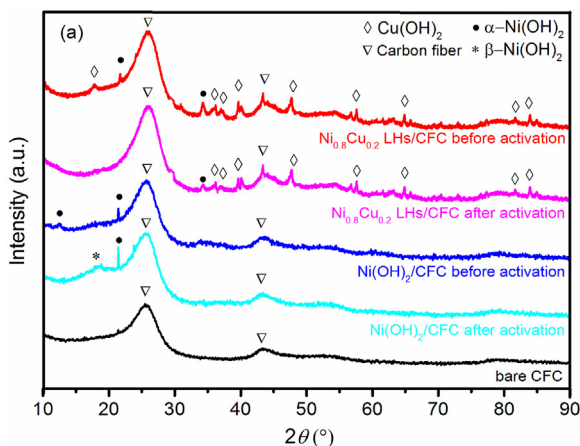


Fig. 2. (a) X-ray diffraction (XRD) patterns of bare CFC, Ni(OH)_2 and $\text{Ni}_{0.8}\text{Cu}_{0.2}$ LHS growing on CFC before and after electrochemical activation. The “ \rightarrow ” indicates Cu(OH)_2 peaks, “●” indicates $\alpha\text{-Ni(OH)}_2$ peaks, “◊” indicates $\beta\text{-Ni(OH)}_2$ and “▽” indicates carbon fibre peaks. (b) The structure change from $\alpha\text{-}(\text{NiOH})_2$ to $\beta\text{-}(\text{NiOH})_2$. Green spheres represent Ni^{2+} ions, blue spheres represent OH^- ions, blue spheres represent H_2O molecules. In $\alpha\text{-}(\text{NiOH})_2$, red spheres represent oxygen, purple spheres represent hydrogen. (c) Ni and (d) Cu XPS spectra of the $\text{Ni}_{0.8}\text{Cu}_{0.2}$ LHS before and after electrocatalytic measurements. (For interpretation of the references to color in this figure legend, the reader is referred to the web version of this article.)

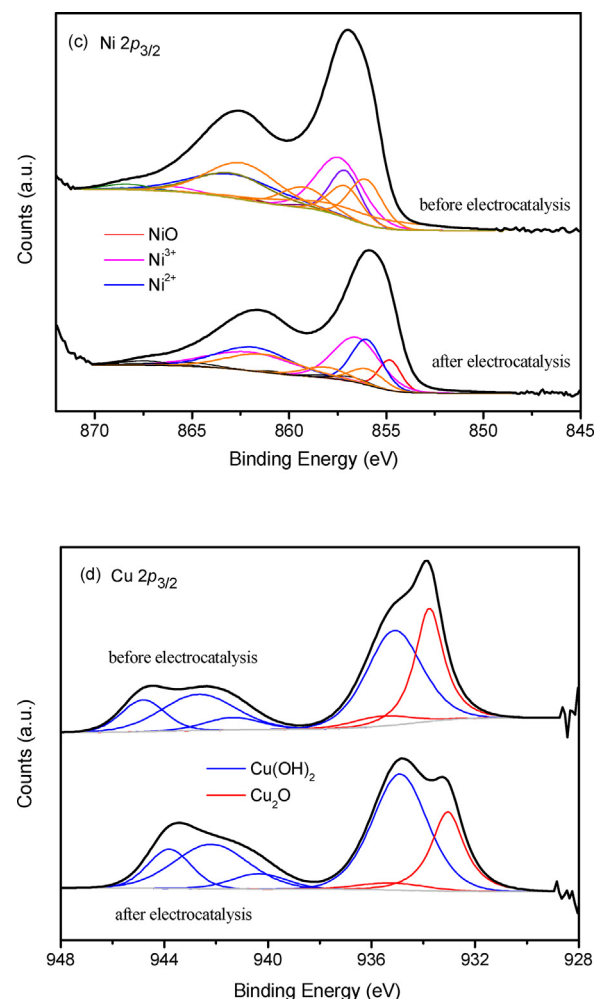


Fig. 2. (Continued))

Compared to the TEM images of hierarchical NiCu LHS nanowires before electrochemical tests (in Fig. S3e and Fig. S3f), hierarchical NiCu LHS were stable to maintain nanowire structure during the electrochemical tests. The presence of crystalline lattice fringes in the high-resolution TEM image (Fig. 3d) with d-spacing value of 0.26 nm might correspond to (110) plane of $\alpha\text{-Ni(OH)}_2$ in the XRD pattern at 2θ of 34° [40], giving additional proof of the hydroxide growth on CFC.

3.2. Electrochemical activity on ammonia oxidation

After electrochemical activation, the prepared samples were used as anodes for electrochemical oxidation of ammonia. Firstly, cyclic voltammetry (CV) measurements of bare hierarchical Ni(OH)_2 and $\text{Ni}_{0.8}\text{Cu}_{0.2}$ LHS catalysts were performed. Both bare Ni(OH)_2 and $\text{Ni}_{0.8}\text{Cu}_{0.2}$ LHS obtained a similar onset potential of ca. 0.43 V vs. Ag/AgCl in pure 0.5 M NaOH aqueous solution (Fig. S4a), this could be attributed to the formation of NiOOH and $\text{Ni}_{0.8}\text{Cu}_{0.2}\text{OOH}$ in reaction (2). Next, CVs were performed in 0.5 M NaOH aqueous solution with the addition of NH_4Cl . As shown in Fig. 4a, the onset potential of ammonia oxidation was in accordance with the formation of $\text{Ni}_{0.8}\text{Cu}_{0.2}\text{OOH}$ as shown in Fig. S4a. At the potential region higher than 0.43 V , the current density of hierarchical $\text{Ni}_{0.8}\text{Cu}_{0.2}$ LHS increased sharply, indicating a high activity toward ammonia electrooxidation. For comparison, the current density of bare Ni(OH)_2 increased gently, much lower than that of $\text{Ni}_{0.8}\text{Cu}_{0.2}$ LHS. It should be emphasized that bare Cu(OH)_2

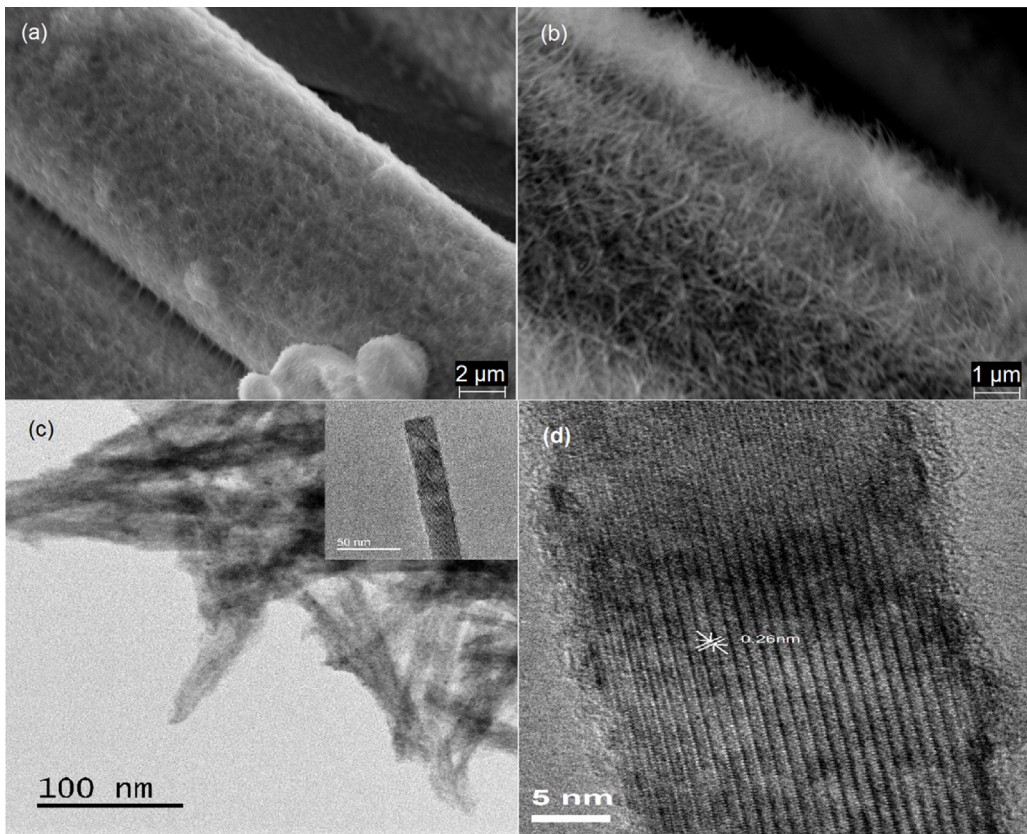


Fig. 3. SEM images of (a) bare $\text{Ni}(\text{OH})_2$ and (b) $\text{Ni}_{0.8}\text{Cu}_{0.2}$ LHs growing on CFC electrode, (c) TEM image of $\text{Ni}_{0.8}\text{Cu}_{0.2}$ LHs after electrochemical measurements with inset of single nanowire; (d) high-resolution TEM image of $\text{Ni}_{0.8}\text{Cu}_{0.2}$ LHs after electrochemical measurements.

presented low activity, which had negligible current response at potential lower than 0.7 V (Fig. S4b). Chronoamperometry tests were performed to measure the stability of the catalysts. As shown in Fig. 4b, the red and blue solid lines represented the observed current density of $\text{Ni}_{0.8}\text{Cu}_{0.2}$ LHs and bare $\text{Ni}(\text{OH})_2$ at 0.55 V vs. Ag/AgCl in 0.5 M NaOH + 55 mM NH_4Cl for a period of 3 h. Bare $\text{Ni}(\text{OH})_2$ reached a current density of only 5 mA cm^{-2} . When doped with Cu, the current density increased 6 times to about 35 mA cm^{-2} . This indicates that the catalytic activity of ammonia electrooxidation was greatly improved by Cu doping. In addition, excellent stability was also shown by the hierarchical $\text{Ni}_{0.8}\text{Cu}_{0.2}$ LHs. Given that the current density observed might be due to the water oxidation reaction taking place in the alkaline condition, chronoamperometry in pure a NaOH electrolyte without NH_4Cl was performed and is shown in Fig. 4b with dotted lines. Under this condition, the current densities of both $\text{Ni}_{0.8}\text{Cu}_{0.2}$ LHs and bare $\text{Ni}(\text{OH})_2$ were very low indicating that the obtained current in the electrolyte of 0.5 M NaOH + 55 mM NH_4Cl was mainly caused by ammonia electrooxidation. Additionally, the chronoamperometry curve of ammonia oxidation by commercial Pt/C is also presented in Fig. S5. The current density achieved from Pt/C was much lower than that from $\text{Ni}_{0.8}\text{Cu}_{0.2}$ LHs, and also decreased gradually (~ 9 to 5 mA cm^{-2}) due to the poisoning of Pt. An activity comparison with other reported catalysts for ammonia electrooxidation are listed in Table S1 of Supporting Information. Compared to reported works, the $\text{Ni}_{0.8}\text{Cu}_{0.2}$ LH nano-wire on carbon fibre cloth exhibits superior activity to electro-oxidation of ammonia.

Linear scan voltammogram (LSV) was used to further investigate the catalytic activities of $\text{Ni}_{0.8}\text{Cu}_{0.2}$ LHs and bare $\text{Ni}(\text{OH})_2$ toward ammonia electrooxidation. As shown in Fig. 5a, a sharp increasing of ammonia oxidation current could be observed above an anode potential of 300 mV. $\text{Ni}_{0.8}\text{Cu}_{0.2}$ LHs achieved much higher current

density at the same applied potential, suggesting that the incorporation of Cu into $\text{Ni}(\text{OH})_2$ could greatly improve the ammonia oxidation performance. The corresponding Tafel plots were measured to evaluate the catalytic kinetics. Fig. 5b exhibits that the Tafel slope of $\text{Ni}_{0.8}\text{Cu}_{0.2}$ LHs catalyst (128 mV dec^{-1}) is smaller than that of bare $\text{Ni}(\text{OH})_2$ catalyst (195 mV dec^{-1}). Hence, under the same conditions the ammonia oxidation reaction could proceed with less electrochemical polarization and facile electron transport on $\text{Ni}_{0.8}\text{Cu}_{0.2}$ LH nano-wire catalyst.

According to the mechanism of ammonia electrooxidation on NiCu LHs catalyst revealed by Reaction (2) and (3), there are three steps: the first one is the formation of $\text{Ni}_{1-x}\text{Cu}_x\text{OOH}$ in alkaline conditions; the second was the adsorption of NH_3 on to $\text{Ni}_{1-x}\text{Cu}_x\text{OOH}$; and the third one was direct electrons lost from NH_3 . Results shown in Fig. 4a & Fig. S4a demonstrate that the onset potential of ammonia oxidation is in accordance with that of $\text{Ni}_{1-x}\text{Cu}_x\text{OOH}$ formation. Thus it was reasonable to believe that the onset potential was dependent on the first step, and the polarization effects in the second and third steps could be negligible. We found that in different concentrations of NaOH solutions ranging from 0.1 M to 6 M the onset potential of $\text{Ni}_{1-x}\text{Cu}_x\text{OOH}$ formation would shift in accordance with Nernst equation. As shown in Fig. S6a, a higher NaOH concentration could lead to a lower onset potential. Similarly, the onset potentials of ammonia electrooxidation also became lower at higher NaOH concentration as shown in Fig. S6b. The onset potentials in 0.1 M, 0.5 M, 2 M, 6 M NaOH solution were about 0.46 V, 0.43 V, 0.36 V, 0.28 V, respectively. Lowering the onset potential is one of the key requirements for reducing energy costs. It was found that the ammonia oxidation current became higher as the NaOH concentration increased from 0.1 M to 2 M (Fig. S6b). However, when the NaOH concentration was further increased to 6 M, the ammonia oxidation current would start to decrease rather than

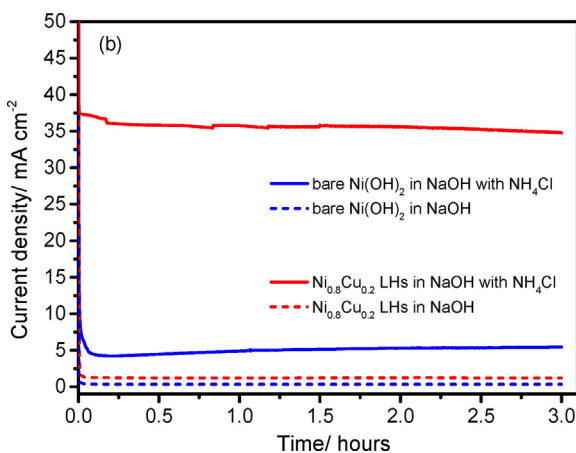
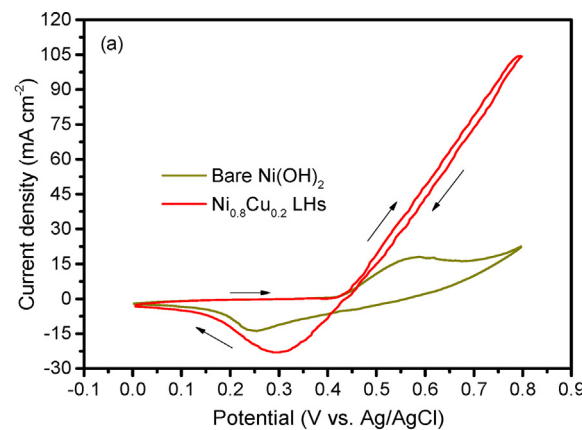


Fig. 4. Catalytic activity and stability. (a) Cyclic voltammetry (CV) of $\text{Ni}_{0.8}\text{Cu}_{0.2}$ LHS and bare $\text{Ni}(\text{OH})_2$ in 0.5 M NaOH + 55 mM NH_4Cl at scan rate of 25 mV s^{-1} at room temperature; (b) chronoamperometry curves at anode potential of 0.55 V vs. Ag/AgCl of $\text{Ni}_{0.8}\text{Cu}_{0.2}$ LHS and bare $\text{Ni}(\text{OH})_2$ in 0.5 M NaOH with and without 55 mM NH_4Cl , respectively. (For interpretation of the references to color in the text, the reader is referred to the web version of this article.)

continuing to increase. This was possibly due to an intense adsorption competition between OH^- and NH_3 occurred at the active sites of the catalysts.

To understand the function of Cu doping on improving catalytic performance, pseudocapacitance of catalysts was calculated from the CV plots in Fig. S4a to evaluate the amounts of active species related to reversible $\text{Ni}_{1-x}\text{Cu}_x(\text{OH})_2/\text{Ni}_{1-x}\text{Cu}_x\text{OOH}$ transformation [31]. The specific capacitance of $\text{Ni}_{0.8}\text{Cu}_{0.2}$ LHS was 902 F g^{-1} , while bare $\text{Ni}(\text{OH})_2$ only had a small capacitance of 280 F g^{-1} , this meant $\text{Ni}_{0.8}\text{Cu}_{0.2}$ LHS has much more active sites when compared to bare $\text{Ni}(\text{OH})_2$. This result could also be attributed to the better morphology of small-sized $\text{Ni}_{0.8}\text{Cu}_{0.2}$ LHS nanowires growing on carbon fibre (Fig. 3b).

To verify this point, samples with different mole ratios of Ni to Cu, named as $\text{Ni}_{1-x}\text{Cu}_x$ LHS were prepared. Their CVs in 0.5 M NaOH solution are shown in Fig. 6a. At increased Cu content the onset potential could be slightly reduced. Specific capacitance of $\text{Ni}_{1-x}\text{Cu}_x$ LHS is summarised in Fig. 6d. When x increased from 0 to 0.2, the value of specific capacitance is also enhanced. However, further increases in x would result in a smaller specific capacitance. This indicates that the $\text{Ni}_{0.8}\text{Cu}_{0.2}$ LHS sample has the largest active surface. Similarly, the $\text{Ni}_{0.8}\text{Cu}_{0.2}$ LHS sample had the largest ammonia oxidation current in CVs (Fig. 6b) and chronoamperometry (Fig. 6c) measurements. In order to avoid the influence of different

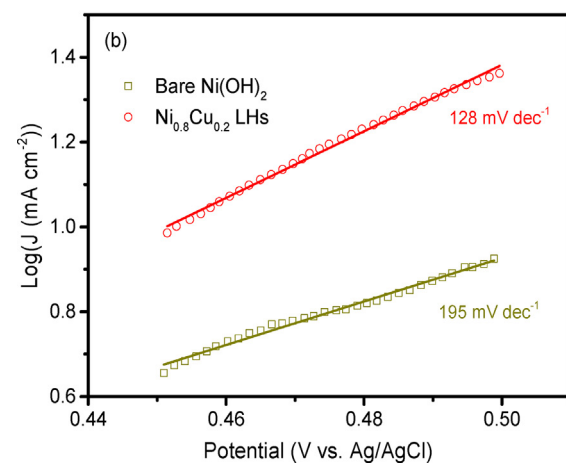
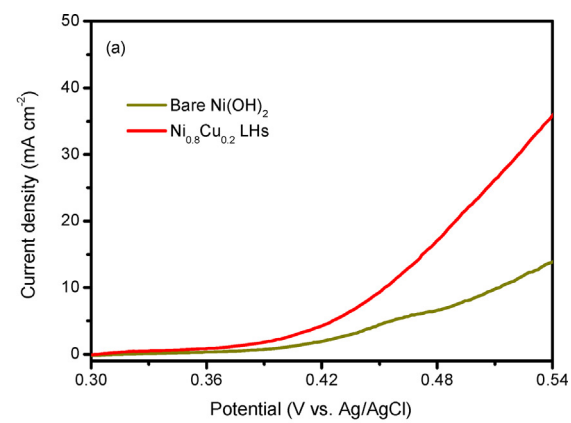


Fig. 5. (a) LSV curves and (b) Tafel plots of $\text{Ni}_{0.8}\text{Cu}_{0.2}$ LHS and bare $\text{Ni}(\text{OH})_2$ in 0.5 M NaOH + 55 mM NH_4Cl .

catalyst loading between these samples, the ammonia oxidation current in Fig. 6c was reproduced as mass current density in Fig. 6d. From $x=0$ to 0.2, the mass current densities reached 2.4 ($x=0$), 18.5 ($x=0.1$), and 22.9 ($x=0.2$) A g^{-1} , respectively. After $x=0.2$, the mass current density decreased to 14.5 ($x=0.3$), 10.5 ($x=0.4$), and 9.3 ($x=0.5$) A g^{-1} , respectively. It is obvious to see that the specific capacitance and catalytic activity had a similar tendency as shown in Fig. 6d. This indicates that the increased active surface after moderate Cu doping could contribute to the enhancement of the ammonia oxidation reaction presented here. In this study, the specific capacity of the NiCu LH catalysts has been shown to correlate to the catalytic activity of electro-oxidation of ammonia. Measured by ionic chromatography, the Ni:Cu molar ratios of NiCu LHS on CFC detected by ion chromatography were 2.4:1, 1.9:1, 1.3:1, 0.78:1 and 0.58:1 for $\text{Ni}_{0.9}\text{Cu}_{0.1}$, $\text{Ni}_{0.8}\text{Cu}_{0.2}$, $\text{Ni}_{0.7}\text{Cu}_{0.3}$, $\text{Ni}_{0.6}\text{Cu}_{0.4}$ and $\text{Ni}_{0.5}\text{Cu}_{0.5}$ LHS, respectively.

3.3. Ammonia electrolysis

A long-time ammonia electrolysis was conducted using 30 mL solution of 50 mM NH_4Cl in 0.1 M NaOH at anode potential of 550 mV in order to verify the ammonia oxidation reaction. The variations of electrolysis currents with time were shown in Fig. S7. An initial current density of $\sim 9 \text{ mA cm}^{-2}$ was achieved by $\text{Ni}_{0.8}\text{Cu}_{0.2}$ LHS, which was twice the value achieved by bare $\text{Ni}(\text{OH})_2$. Then the electrolysis currents of both $\text{Ni}_{0.8}\text{Cu}_{0.2}$ LHS and bare $\text{Ni}(\text{OH})_2$ decreased gradually due to the consumption of ammonia in solution. The concentrations of ammonia and nitrate ions in the

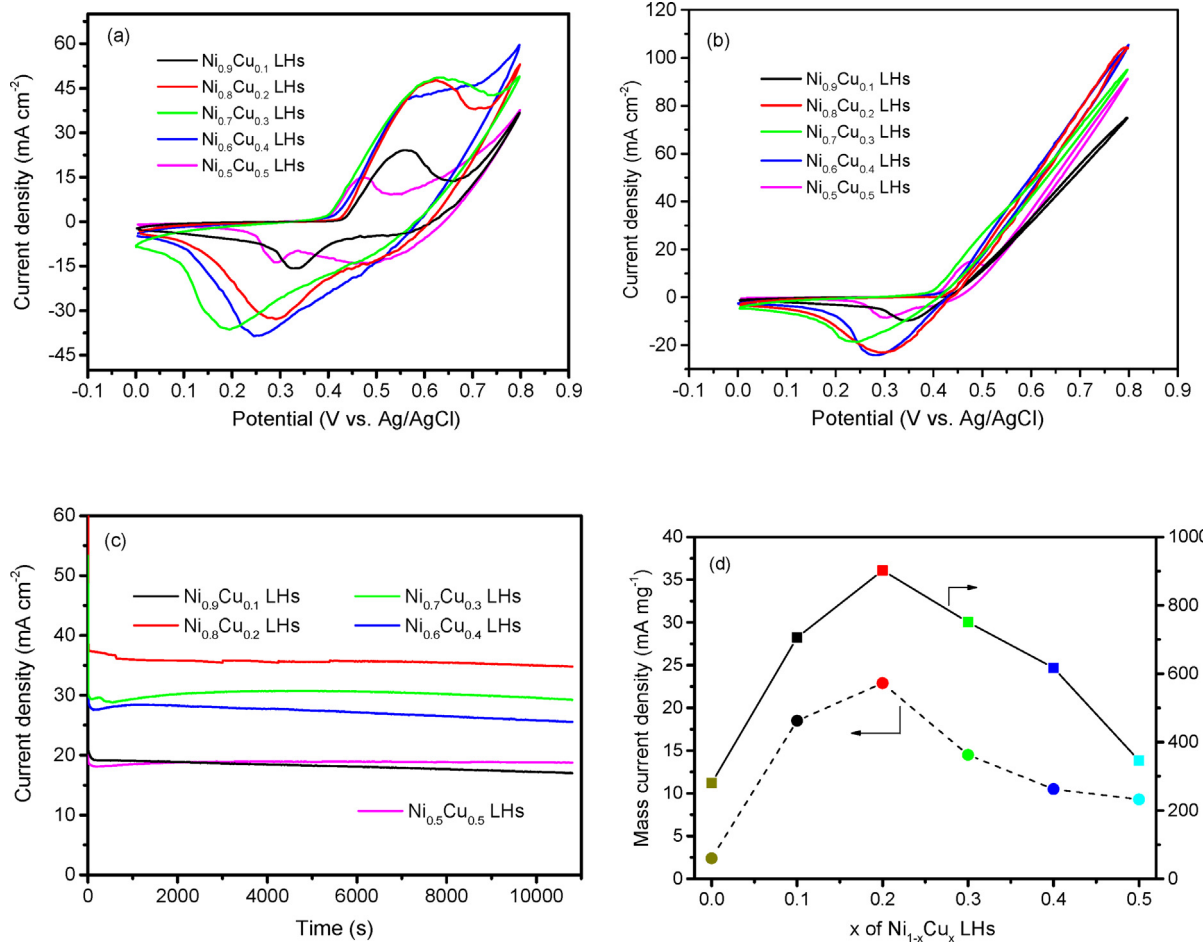


Fig. 6. CVs of $\text{Ni}_{1-x}\text{Cu}_x$ ($x=0.1, 0.2, 0.3, 0.4, 0.5$) LHSs in (a) 0.5 M NaOH and (b) in 0.5 M NaOH with 55 mM NH_4Cl at scan rate of 25 mV s⁻¹ at room temperature; (c) chronoamperometry curves at anode potential of 0.55 V vs. Ag/AgCl of $\text{Ni}_{1-x}\text{Cu}_x$ ($x=0.1, 0.2, 0.3, 0.4, 0.5$) LHSs in 0.5 M NaOH with 55 mM NH_4Cl ; (d) The relations between x of $\text{Ni}_{1-x}\text{Cu}_x$ LHSs and mass current density as well as specific capacitance.

Table 1
NH₃ and NO- 3 concentrations during long-time ammonia electrolysis.

Catalysts	Concentrations of NH ₃ (mM)			Concentrations of NO- 3 (mM)		
	At 0 h	At 9 h	At 24 h	At 0 h	At 9 h	At 24 h
$\text{Ni}(\text{OH})_2$	50	30.6	21.2	0	7.2	8.5
$\text{Ni}_{0.8}\text{Cu}_{0.2}$ LHSs	50	17.8	8.1	0	8.5	11.6

electrolysis solution are listed in Table 1. Ammonia concentration was reduced during electrolysis with a final removal efficiency of 58% for $\text{Ni}(\text{OH})_2$ and 84% for $\text{Ni}_{0.8}\text{Cu}_{0.2}$ LHSs. This demonstrates that a faster rate of ammonia oxidation could be obtained for the hierarchical $\text{Ni}_{0.8}\text{Cu}_{0.2}$ LHSs catalyst compared to $\text{Ni}(\text{OH})_2$ catalyst. Nitrite ions were not detected in this work, the possible reason might be that nitrite ions were oxidized to nitrate ions rapidly. Nitrite ions can be oxidized to nitrate ions by oxygen dissolved in the electrolyte solution [43]. Under suitable conditions, nitrite ions can be electro-oxidized to nitrate ions as well [44]. The Ni/Cu ratio before and after electrolysis did not change, which was 1.9:1 according to ion chromatography measurement. No Ni^{2+} or Cu^{2+} was determined in the electrolyte after electrolysis tests. The anodic coulombic efficiency (η_a) was calculated according to the following equation based on NH₃ oxidation:

$$\eta_a = \frac{Q_e}{Q_t} = \frac{nFV(C_0 - C_t)/1000}{\int I dt} \quad (4)$$

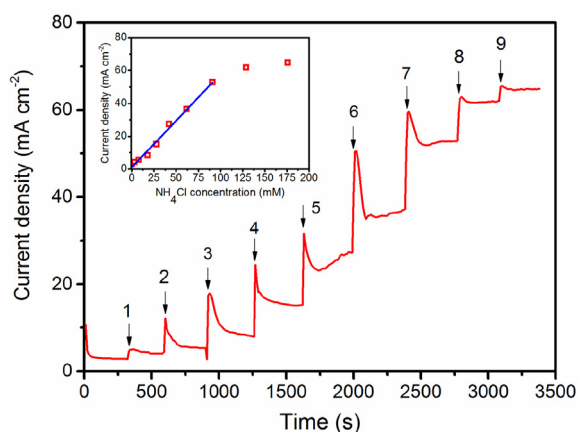


Fig. 7. The current response of $\text{Ni}_{0.8}\text{Cu}_{0.2}$ LHSs to step-by-step injections of NH₄Cl solution (marked by arrows and numbers) to 1 M NaOH at room temperature; Anode potential 0.55 V vs. Ag/AgCl. The inset plot showed the current density as a function of ammonia concentration in solution for the 9 injections.

Where Q_t was the total consumed electric quantity calculated from the integral discharge current-time curve in Fig. S7, and Q_e was theoretically transferred electric quantities from NH₃ oxidation; C_0 and C_t were initial and final ammonia concentration (mM), respectively; V , F , n were electrolyte volume (30 mL), Faraday constant (96,485 C mol⁻¹) and transferred electron number (3). The η_a at

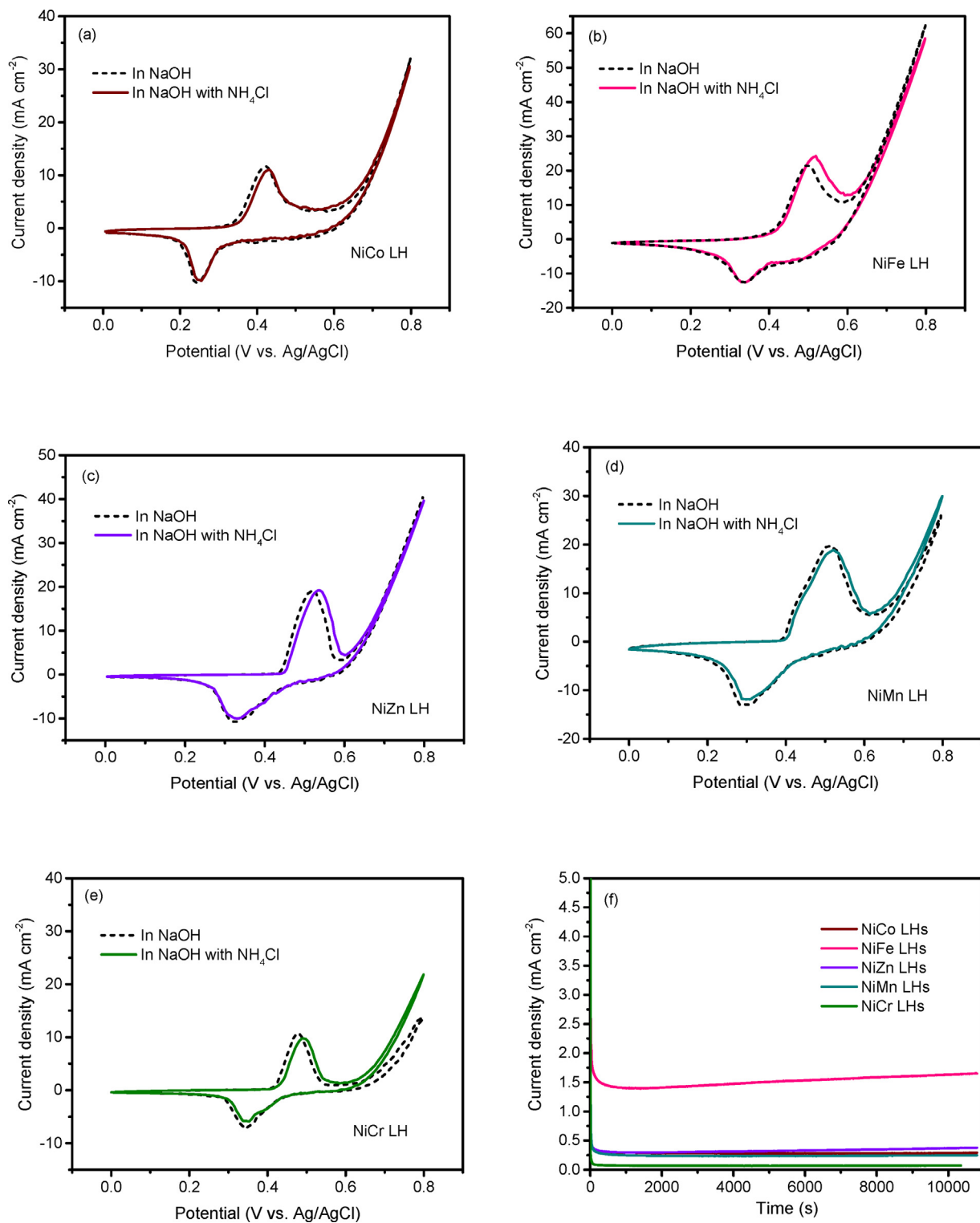
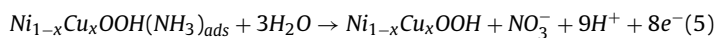


Fig. 8. CVs of (a) NiCo LH; (b) NiFe LH; (c) NiZn LH; (d) NiMn LH; (e) NiCr LH in 0.5 M NaOH with and without 55 mM NH₄Cl at a scan rate of 25 mV s⁻¹ at room temperature; (f) chronoamperometry curves of NiM LHs at anode potential of 0.55 V vs. Ag/AgCl in 0.5 M NaOH with 55 mM NH₄Cl.

24 h were 64.9% and 62.5% for Ni(OH)₂/CFC and Ni_{0.8}Cu_{0.2}/CFC electrodes, respectively. The obtained η_a was not very high possibly because of that only a small portion of ammonia was oxidized to nitrate; this was perhaps the result of the oxygen transfer reaction between water and ammonia molecules:



3.4. Influence of ammonia concentration on the catalytic activity

The effect of ammonia concentration on the catalytic activity was also investigated at different concentrations. Ammonia concentration was changed from 0 to 180 mM in 1 M NaOH, with the current response recorded in Fig. 7. The oxidation current was observed to increase linearly when the ammonia concentration was increased from 0 to 91 mM. This indicates that the current

was mainly limited by mass transfer in the electrolyte. The current continues to increase as concentration was further increased from 91 mM to 180 mM, thereby demonstrating that Ni_{0.8}Cu_{0.2} LHs does not deactivate at high ammonia concentrations. At ammonia concentration higher than 130 mM, the increase of oxidation current seems to slow down, this is probably due to the saturation of the active sites on Ni_{0.8}Cu_{0.2} LHs. This indicates Ni_{0.8}Cu_{0.2} LHs can be used as anode for electrolysis of ammonia in wastewater when a high concentration of ammonia is presented.

3.5. Activity of various Ni-based LHs

The choice of doping elements is vitally important in order to improve catalysts activity. First-row transition metals have been widely used as doping elements to prepare Ni-based layered hydroxides. Apart from NiCu LHs, other NiM LHs compositions were also investigated in this work. These were NiCo, NiFe, NiZn, NiMn and NiCr. Cyclic voltammetry and chronoamperometry were used to measure their electrochemical activity toward ammonia oxidation reaction and shown in Fig. 8a–f. Nevertheless, these results are totally different when compared with those obtained for NiCu LHs. All five types of NiM LHs (M=Co, Fe, Zn, Mn, Cr) had almost no response to ammonia oxidation although the same activation process was carried out. CV plots show that there is no significant differences with the absence and presence of NH₄Cl, indicating that the NiM LHs (where M=Co, Fe, Zn, Mn, Cr) were inactive toward ammonia electrooxidation. This was further demonstrated by the data in Fig. 8f. The oxidation current densities of NiCo, NiZn, NiMn and NiCr LHs were all less than 0.5 mA cm⁻². The current density of NiFe LH was relative high compared to other NiM LHs, reaching about 1.5 mA cm⁻². However, this current was most probably caused by water oxidation, as NiFe LH is a state-of-the-art catalyst for water oxidation with low overpotential. Please note that an ammonia oxidation current of about 5 mA cm⁻² has been achieved by using bare Ni(OH)₂ (Fig. 4b), this value is much higher than all the values presented in Fig. 8f. In another word, when doped with Co, Fe, Zn, Mn or Fe elements, the activity of Ni(OH)₂ would be reduced rather than improved. Further investigation is required to understand the mechanism behind.

Among the investigated transition elements, Cu proved unique in its ability to improve the activity of Ni(OH)₂ for ammonia electrooxidation. The increased active surface area of catalysts cannot be the only reason ascribed to the distinctive effect of Cu. Another reason might be the intrinsic catalytic activity of NiCu LHs. According to first-principles study, of the metals with activity for ammonia electrooxidation, Cu was among the highest [32]. However, it has been reported that Cu itself was not able to oxidize ammonia, as it performed poorly in the adsorption of NH₃ [33]. On the other hand, Ni has a strong adsorption of NH₃ [32]. Thus the combination of Cu and Ni might have synergistic effects making it easier to form Ni_{1-x}Cu_xOOH(NH₃)_{ads} due to Ni therefore making the oxidation reaction faster than that for Cu. The electrochemical activation process to convert Cu(OH)₂ and α-Ni(OH)₂ into Ni_{1-x}Cu_xOOH is a crucial step to achieve high activity towards electrochemical oxidation of ammonia.

4. Conclusions

In conclusion, hierarchical NiCu LHs nanowires have been successfully grown directly on carbon fibre cloth by a hydrothermal reaction followed by electrochemical activation. The as-prepared hierarchical NiCu LH nano-wire showed superior catalytic activity towards ammonia electrooxidation when compared to bare Ni(OH)₂ and commercial Pt/C catalysts. This activity improvement was mainly attributed to abundant active sites and the synergistic

effect of Ni and Cu due to the possible formation of Ni_{1-x}Cu_xOOH during the electrochemical activation process. In our study it was revealed that Cu was unique in the investigated first-row transition metals as the only element which could enhance the activity of Ni(OH)₂. The optimised Cu doping level was 20 mol% at the starting precursor with a real Ni to Cu molar ratio of 1.9:1. Unlike the Pt catalyst, the hierarchical NiCu LHs nano-wire did not deactivated and was stable at high ammonia concentration, as well as being a lot less expensive. With these properties, Cu incorporated Ni-based LHs nano-wire could be a promising stable and low-cost catalyst for efficient electrooxidation of ammonia. This kind of materials has the potential to be used as efficient electrode for ammonia fuel cells for power generation or electrolysis of ammonia for ammonia-containing wastewater treatment.

Acknowledgments

The authors thank EPSRC for funding (Grant No. EP/G01244X/1). One of the authors (Xu) gratefully acknowledges the China Scholarship Council (CSC) for financial support.

Appendix A. Supplementary data

Supplementary data associated with this article can be found, in the online version, at <http://dx.doi.org/10.1016/j.apcatb.2017.07.005>.

References

- [1] N.V. Rees, R.G. Compton, Energy Environ. Sci. 4 (2011) 1255–1260.
- [2] R. Lan, J.T.S. Irvine, S.W. Tao, Int. J. Hydrogen Energy 37 (2012) 1482–1494.
- [3] F. Schuth, R. Palkovits, R. Schlogl, D.S. Su, Energy Environ. Sci. 5 (2012) 6278–6289.
- [4] M.H.M.T. Assumpção, R.M. Piasentini, P. Hammer, R.F.B. De Souza, G.S. Buzzo, M.C. Santos, E.V. Spinacé, A.O. Neto, J.C.M. Silva, Appl. Catal. B: Environ. 174–175 (2015) 136–144.
- [5] D.J. Little, I.I.M.R. Smith, T.W. Hamann, Energy Environ. Sci. 8 (2015) 2775–2781.
- [6] T. Okanishi, Y. Katayama, H. Muroyama, T. Matsui, K. Eguchi, Electrochim. Acta 173 (2015) 364–369.
- [7] J. Yang, A.F.S. Molouk, T. Okanishi, H. Muroyama, T. Matsui, K. Eguchi, ACS Appl. Mater. Interfaces 7 (2015) 7406–7412.
- [8] A. Estejab, D.A. Daramola, G.G. Botte, Water Res. 77 (2015) 133–145.
- [9] A. Ponrouch, S. Garbarino, E. Bertin, C. Andrei, G.A. Botton, D. Guay, Adv. Funct. Mater. 22 (2012) 4172–4181.
- [10] G.-T. Fu, C. Liu, R. Wu, Y. Chen, X.-S. Zhu, D.M. Sun, Y.-W. Tang, T.-H. Lu, J. Mater. Chem. A 2 (2014) 17883–17888.
- [11] J. Liu, B. Chen, Y. Kou, Z. Liu, X. Chen, Y. Li, Y. Deng, X. Han, W. Hu, C. Zhong, J. Mater. Chem. A 4 (2016) 11060–11068.
- [12] S. Le Vot, L. Roué, D. Bélanger, J. Power Sources 223 (2013) 221–231.
- [13] Z. Ni, J. Liu, Y. Wu, B. Liu, C. Zhao, Y. Deng, W. Hu, C. Zhong, Electrochim. Acta 177 (2015) 30–35.
- [14] L. Cunci, C.A. Velez, I. Perez, A. Suleiman, E. Larios, M. José-Yacamán, J.J. Watkins, C.R. Cabrera, ACS Appl. Mater. Interfaces 6 (2014) 2137–2145.
- [15] C. Zhong, W.B. Hu, Y.F. Cheng, J. Mater. Chem. A 1 (2013) 3216–3238.
- [16] K. Yao, Y.F. Cheng, J. Power Sources 173 (2007) 96–101.
- [17] K. Yao, Y.F. Cheng, Mater. Chem. Phys. 108 (2008) 247–250.
- [18] A. Kapałka, A. Cally, S. Neodo, C. Comninellis, M. Wächter, K.M. Udert, Electrochim. Commun. 12 (2010) 18–21.
- [19] W. Xu, H. Zhang, G. Li, Z. Wu, Sci. Rep. 4 (2014) 5863.
- [20] W. Xu, Z. Wu, S.W. Tao, Energy Technol. 4 (2016) 1329–1337.
- [21] J. Jiang, L. Huang, X. Liu, L. Ai, ACS Appl. Mater. Interfaces 9 (2017) 7193–7201.
- [22] T. Tian, J. Jiang, L. Ai, Electrochim. Acta 224 (2017) 551–560.
- [23] M. Jing, H. Hou, C.E. Banks, Y. Yang, Y. Zhang, X. Ji, ACS Appl. Mater. Interfaces 7 (2015) 22741–22744.
- [24] O. Diaz-Morales, I. Ledezma-Yanez, M.T.M. Koper, F. Calle-Vallejo, ACS Catal. 5 (2015) 5380–5387.
- [25] C. Qiu, J. Jiang, L. Ai, ACS Appl. Mater. Interfaces 8 (2016) 945–951.
- [26] X. Yu, M. Zhang, W. Yuan, G. Shi, J. Mater. Chem. A 3 (2015) 6921–6928.
- [27] L. Huang, J. Jiang, L. Ai, ACS Appl. Mater. Interfaces 9 (2017) 7059–7067.
- [28] K. Fan, H. Chen, Y. Ji, H. Huang, P.M. Claesson, Q. Daniel, B. Philippe, H. Rensmo, F. Li, Y. Luo, L. Sun, Nat. Commun. 7 (2016) 11981.
- [29] S. Klaus, Y. Cai, M.W. Louie, L. Trotocaud, A.T. Bell, J. Phys. Chem. C 119 (2015) 7243–7254.
- [30] L. Trotocaud, S.L. Young, J.K. Ranney, S.W. Boettcher, J. Am. Chem. Soc. 136 (2014) 6744–6753.

- [31] W. Xu, D.W. Du, R. Lan, J. Humphreys, D.N. Miller, M. Walker, Z.C. Wu, J.T.S. Irvine, S.W. Tao, *Appl. Catal. B: Environ.* (2017), <http://dx.doi.org/10.1016/j.apcatb.2016.1011.1003>.
- [32] J.A. Herron, P. Ferrin, M. Mavrikakis, *J. Phys. Chem. C* 119 (2015) 14692–14701.
- [33] A.C.A. de Vooys, M.T.M. Koper, R.A. van Santen, J.A.R. van Veen, *J. Electroanal. Chem.* 506 (2001) 127–137.
- [34] L.L. Wang, X.D. Duan, G.M. Wang, C.B. Liu, S.L. Luo, S.Q. Zhang, Y.X. Zeng, Y.Z. Xu, Y.T. Liu, X.F. Duan, *Appl. Catal. B-Environ.* 186 (2016) 88–96.
- [35] P. Trogadas, V. Ramani, P. Strasser, T.F. Fuller, M.-O. Coppens, *Angew. Chem. Int. Ed.* 55 (2016) 122–148.
- [36] R. Lan, J.T.S. Irvine, S.W. Tao, *Sci. Rep.* 3 (2013) 1145.
- [37] D.W. Du, R. Lan, W. Xu, R. Beanland, H.T. Wang, S.W. Tao, *J. Mater. Chem. A* 4 (2016) 17749–17756.
- [38] K.I. Pandya, W.E. O'Grady, D.A. Corrigan, J. McBreen, R.W. Hoffman, *J. Phys. Chem.* 94 (1990) 21–26.
- [39] J. Jiang, C. Zhang, L. Ai, *Electrochim. Acta* 208 (2016) 17–24.
- [40] M.C. Biesinger, B.P. Payne, A.P. Grosvenor, L.W.M. Lau, A.R. Gerson, R.S. Smart, *Appl. Surf. Sci.* 257 (2011) 2717–2730.
- [41] R.S. McEwen, *J. Phys. Chem.* 75 (1971) 1782–1789.
- [42] D.S. Hall, D.J. Lockwood, C. Bock, B.R. MacDougall, *Proc. R. Soc. A: Math. Phys. Eng. Sci.* 471 (2015) 20140792.
- [43] A. Pollice, V. Tandoi, C. Lestangi, *Water Res.* 36 (2002) 2541–2546.
- [44] F. Armijo, M.C. Goya, M. Reina, M.J. Canales, M.C. Arévalo, M.J. Aguirre, *J. Mol. Catal. A: Chem.* 268 (2007) 148–154.